

RESEARCH

Open Access



Lack of neuroinflammation in the HIV-1 transgenic rat: an [^{18}F]-DPA714 PET imaging study

Dianne E. Lee¹, Xuyi Yue², Wael G. Ibrahim¹, Margaret R. Lentz¹, Kristin L. Peterson¹, Elaine M. Jagoda³, Michael Kassiou⁴, Dragan Maric⁵, William C. Reid¹ and Dima A. Hammoud^{1*}

Abstract

Background: HIV-associated neuroinflammation is believed to be a major contributing factor in the development of HIV-associated neurocognitive disorders (HAND). In this study, we used micropositron emission tomography (PET) imaging to quantify neuroinflammation in HIV-1 transgenic rat (Tg), a small animal model of HIV, known to develop neurological and behavioral problems.

Methods: Dynamic [^{18}F]DPA-714 PET imaging was performed in Tg and age-matched wild-type (WT) rats in three age groups: 3-, 9-, and 16-month-old animals. As a positive control for neuroinflammation, we performed unilateral intrastriatal injection of quinolinic acid (QA) in a separate group of WT rats. To confirm our findings, we performed multiplex immunofluorescent staining for Iba1 and we measured cytokine/chemokine levels in brain lysates of Tg and WT rats at different ages.

Results: [^{18}F]DPA-714 uptake in HIV-1 Tg rat brains was generally higher than in age-matched WT rats but this was not statistically significant in any age group. [^{18}F]DPA-714 uptake in the QA-lesioned rats was significantly higher ipsilateral to the lesion compared to contralateral side indicating neuroinflammatory changes. Iba1 immunofluorescence showed no significant differences in microglial activation between the Tg and WT rats, while the QA-lesioned rats showed significant activation. Finally, cytokine/chemokine levels in brain lysates of the Tg rats and WT rats were not significantly different.

Conclusion: Microglial activation might not be the primary mechanism for neuropathology in the HIV-1 Tg rats. Although [^{18}F]DPA-714 is a good biomarker of neuroinflammation, it cannot be reliably used as an *in vivo* biomarker of neurodegeneration in the HIV-1 Tg rat.

Keywords: HIV, Transgenic rat, Positron emission tomography, Neuroinflammation

Background

In the developed world where antiretroviral therapy (ART) is readily available, HIV/AIDS has been transformed from a once fatal to a chronic manageable disease, with markedly decreased mortality and morbidity. Along the same lines, the incidence of severe neurocognitive dysfunction decreased significantly [1]. The more subtle forms of neurocognitive dysfunction

however became more prevalent, leading to gradual, but ultimately significant functional deterioration of otherwise virologically controlled HIV+ patients [2].

Among various factors, the contribution of neuroinflammation/microglial activation to neuronal damage in HIV is assumed to play a major role [3] based on multiple cell culture studies [4–7] as well as direct histological evaluation of brain tissues from untreated HIV or simian immunodeficiency virus-infected animals [8]. The hallmark of neuroinflammation is the activation of naturally quiescent resident microglial cells [9] resulting in the unregulated secretion of multiple neurotoxins and cytotoxins, ultimately resulting in neuronal damage leading to cell death [3, 10]. The ability to

* Correspondence: hammoudd@cc.nih.gov

¹Center for Infectious Disease Imaging (CIDI), Radiology and Imaging Sciences, National Institutes of Health/Clinical Center, 10 Center Drive, Room 1C368, Bethesda, MD 20814-9692, USA

Full list of author information is available at the end of the article

non-invasively monitor neuroinflammation is thus an important target in the diagnosis, prevention, and evaluation of treatment effect in many neurological diseases including neuro-HIV.

Imaging microglial activation as a surrogate marker for neuroinflammation can be done through the use of specific radiolabeled ligands targeting the translocator protein (TSPO, previously known as the peripheral benzodiazepine receptor (PBR)) [3], an 18 kD outer mitochondrial membrane receptor which is naturally expressed in small amounts in resting microglial cells. TSPO however gets significantly upregulated during microglial activation [9]. The prototype positron emission tomography (PET) TSPO ligand, [^{11}C]PK11195, has been extensively used to image neuroinflammation in a variety of neurodegenerative diseases [11–16] but has long been criticized for inherent limitations such as high non-specific binding and high lipophilicity [17–20]. Newer higher affinity ligands for TSPO, such as DPA-713 [21], PBR-28 [22], CLINDE [23, 24], and DAA [25], among others, have been developed as a result.

In this study, we set out to validate one of the newly designed TSPO ligands, [^{18}F]DPA-714, an ^{18}F -labeled pyrazolopyrimidine, [19, 20, 26], as surrogate imaging biomarker of microglial activation (neuroinflammation), *in vivo*, in the brains of HIV-1 transgenic rats (Tg) compared to age-matched controls. We wanted to test the hypothesis that the Tg rat brain shows microglial activation which would potentially allow the use of [^{18}F]DPA-714 PET in this animal model as a biomarker for the effectiveness of various neuroprotective/anti-inflammatory therapies.

Methods

Animals

Experiments were carried out in male Tg (F344/Hsd) in three different age groups (3, 9, and 16 month-old) and male age-matched wild-type control rats (F344) (WT) purchased from Harlan Inc. (Indianapolis, IN). The total sample of animals used for PET imaging, blood metabolism experiments, and cytokine/chemokine measurements included 28 Tg and 27 WT rats. All rats were housed in a temperature-controlled environment with a 12-h light/dark cycle. The animals were allowed free access to food and water. All procedures were conducted during the light cycle. The rats were acclimated to careful handling prior to testing to minimize stress. Animal care and all experimental procedures were approved by the Institutional Animal Care and Use Committee (ACUC) of the National Institutes of Health (NIH).

QA surgical procedures

Three WT rats weighing 210 ± 114 g were used for intrastriatal injection of quinolinic acid (QA). The animals were

anesthetized with 1 mg/kg ketamine and xylazine (10:1) cocktail (Sigma) and then placed in a stereotaxic apparatus (Stoelting Wood Dale, IL, USA). Unilateral stereotaxic injections of 150 nmol in 1 μl of QA (Sigma; dissolved in 0.1 M phosphate-buffered saline (PBS), pH 7.4) in the right striatum were made over 5 min using a 10 μl Hamilton syringe fitted with a micropump (Stoelting Wood Dale, IL, USA). The syringe was fitted with a 26-gauge needle at the following coordinates according to Paxinos and Watson (1998): anteroposterior (AP) +1 mm, mediolateral (ML) –3.0 mm, dorsoventral (DV) –4.5 mm, from the bregma. The injection syringe was left in place for an additional 5 min to allow the QA to diffuse from the needle tip and avoid backflow. After removing the needle, the skin was sutured and the animals were allowed to recover before being returned to their cages. The animals were given buprenorphine (0.03 mg/kg) intramuscularly and examined daily until PET imaging. PET imaging studies were conducted either 7 days post-op ($n = 1$) or 3 days post-op ($n = 2$). All animal procedures were performed in accordance with the NIH ACUC guidelines.

Radiochemistry

Automated syntheses of [^{18}F]DPA-714 were carried out using a slightly modified TRACERLab FX-FN module (GE Medical Systems, Germany). In brief, aqueous [^{18}F]fluoride anions were sucked through the Chroma-fix[®] under vacuum. The trapped ^{18}F -fluoride was eluted from the cartridge and transferred to the reaction vessel with an eluent solution containing K_2CO_3 , acetonitrile, and Kryptofix-222. The reaction mixture was evaporated to dryness after addition. Tosylate substrate was then dissolved in dimethyl sulfoxide, and the mixture was transferred to the dry ^{18}F -labeled KF-K222 complex and allowed to react at 165 $^\circ\text{C}$ for 5 min. On completion, the reaction mixture was diluted with semi-preparative HPLC solvent and passed through a Sep-Pak[®] light Alumina N cartridge (Waters Corporation, Milford, MA). The reaction vessel was rinsed with HPLC solvent and passed through the Sep-Pak[®] Alumina N cartridge by helium pressure. The combined crude solution collected in the collection flask was transferred to the HPLC injection loop and injected into a Phenomenex Luna 5 μm C18 semi-preparative reversed-phase HPLC column (250 \times 10 mm), with a mobile phase of H_2O and acetonitrile (55/45, *v/v*) at a flow rate of 4.0 ml/min. The retention time (tR) of [^{18}F]DPA-714 was determined to be 19 min. The radioactive fraction corresponding to [^{18}F]DPA-714 was collected into a dilution flask. The final formulation of the tracer was performed automatically using a Sep-Pak[®] Plus C18-based system. The diluted fraction collected from the dilution flask was passed through the C18 cartridge to fix the tracer. The cartridge was washed with deionized water (10 ml), and the purified

tracer was finally recovered by elution of the C18 cartridge with the ethanol (1.5 ml) from the reservoir. Yield and specific activity were determined at this stage (25 ± 3 %, specific activity $41\text{--}107$ GBq/ μmol , $n > 10$). The excess ethanol was removed through rotary evaporation and concentrated to $250\text{--}350$ μl . The tracer was delivered and diluted with PBS for final formulation and animal administration.

[^{18}F]DPA-714 blood metabolism

The Tg ($n = 3$, 10 ± 1 months) and age-matched WT rats ($n = 3$, 10 ± 0.5 months) were anesthetized with 2–2.5 % isoflurane air/oxygen mixture and injected with 1–2 mCi ($37\text{--}74$ MBq) of [^{18}F]DPA-714 (1.65 ± 0.43 mCi; 61.05 ± 15.91 MBq). Aliquots of blood (400 μl) were taken from each animal at 5, 15, 30, and 60 min post-injection and centrifuged at $17,000\times g$ at 4°C for 4 min. One hundred microliter of plasma was retrieved, and extraction was performed using 200- μl acetonitrile. The mixture was vortexed for 30 s and centrifuged at $17,000\times g$, 4°C for 4 min. The supernatant was removed and 25 μl from each sample was applied on silica gel thin layer chromatography (TLC) plates. A mixture of chloroform (90%), methanol (9%), and ammonium hydroxide (1%) was used as the eluent. The dried TLC plates were placed overnight on a phosphorimaging plate with a pixel size of 25 μm (Fuji BAS-SR2025, Fujifilm, Japan). After exposure, the plates were scanned using a Fuji FLA-5100 and the data was analyzed using Image Gauge (Fujifilm, Japan). The radioactivity of the remaining plasma and pellets was determined by γ -counting (Perkin Elmer 2480 Wizard3)

and used to calculate the percent parent uptake of the plasma, corrected for metabolites (differential uptake ratio, DUR = % injected dose normalized to animal weight and plasma volume). Finally, the percentages of unchanged [^{18}F]DPA-714 in plasma as a function of time were fitted to an exponential decay equation (Fig. 1).

[^{18}F]DPA-714 PET

The 3-month-old group consisted of four Tg (237 ± 46 g) and four age-matched WT rats (263 ± 27 g). The 9-month-old group consisted of five Tg (344 ± 36 g) and five WT rats (410 ± 41 g). The 16-month-old group consisted of six Tg (392 ± 25 g) and three WT rats (464 ± 11 g).

Two to three rodents were scanned per day, and the order of scanning was counterbalanced: one Tg rat and one WT rat, in alternate order. The animals were anesthetized with 2–2.5 % isoflurane air/oxygen mixture. The intra-subject variability of the depth of anesthesia was monitored by measuring respiratory frequency periodically during the scan. The PET experiments were performed on a Bio PET/CT tomograph (Bioscan Inc., Washington, DC) with an axial field of view of 4.8 and 6.7 cm in diameter. Time coincidence window was set to 10 ns with an energy window of 250–700 keV. The lateral tail vein was cannulated for injection of radio-tracer, and the cannula was then connected to a heparin lock and secured in place with medical tape. The animal was positioned prone with the head placed symmetrically in the center field of view (FOV) on the thermostatically heated bed supplied by the manufacturer (Bioscan Inc., Washington, DC).

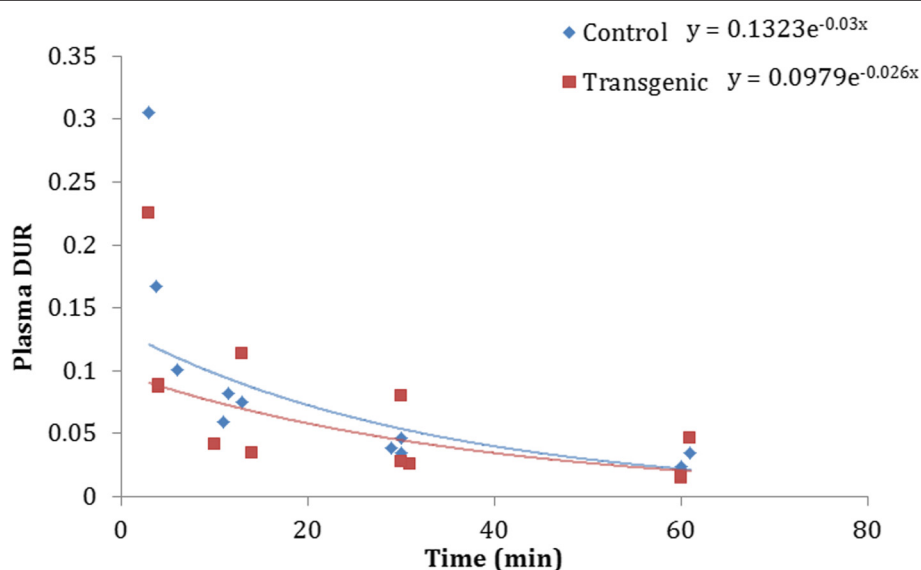


Fig. 1 [^{18}F]DPA-714 plasma metabolism in WT and Tg 10-month-old rats over 60 min. Blood samples were collected at four time points per animal. The Tg ($t_{1/2} = 23.10$ min) and WT rats ($t_{1/2} = 26.66$ min) had similar patterns of metabolism. DUR differential uptake ratio = % injected dose normalized to animal weight and plasma volume)

[^{18}F]DPA-714 injection of 1.66 ± 0.22 mCi (61.4 ± 8.1 MBq; 2.0 ± 0.9 nmol/rat) was then administered as a bolus injection (30 s) into the indwelling intravenous catheter followed by a 300- μl saline flush (maximum volume of injection = 600 μl). PET emission data was acquired for 60 min in list mode and then reframed into a dynamic sequence of 20 frames (6×20 , 3×60 , 11×300). The resultant emission Sinogram for each frame were then corrected for attenuation, scatter, ^{18}F decay, randoms, and dead time. Dynamic images were reconstructed using OSEM-2D algorithm into $175 \times 175 \times 61$ slices with a voxel size of $0.39 \times 0.39 \times 0.78$ mm. The reconstructed images were co-registered to a template MR in stereotaxic space using a rigid body transformation model as previously described [27]. Time-activity curves were generated for volumes of interest (VOIs) that were drawn manually on the template MR image guided by an anatomical atlas of the rodent brain [28]. The VOI positions were evaluated by displaying the corresponding VOI on the co-registered PET images. Image analyses were performed using PMOD 3.4 kinetic modeling tool (PMOD Technologies Ltd., Zurich, Switzerland). Regional [^{18}F]DPA-714 uptake was quantified as standardized uptake value equivalent to percentage of injected dose per cubic centimeter after correction for body weight ($\text{SUV}_c = \% \text{ID kg/cm}^3$). The SUVs were calculated from the imaging frames obtained between 40 and 60 min after injection. Those frames were assumed to reflect “pseudo equilibrium” status since they had the lowest rate of change in the concentration activity curve ($<5\%$ /h) [29]. The body weight was adjusted according to Kleiber laws [30] as previously described [31] to account for weight differences between our adult Tg and adult WT rat. For the QA injection group, we calculated the ratio of uptake in the ipsilateral striatum (site of injection) and cortex (needle track) to the contralateral striatum and cortex (reference region).

Immunofluorescence

Tissue preparation

The Tg rats ($n = 14$) and WT rats ($n = 12$), ranging in age from 1 to 10 months, were first anesthetized with isoflurane (3 % with 700 cc/min O_2). This was followed by transcardial perfusion using 100 ml of normal saline (pH = 7.4) and 350 ml of freshly prepared and filtered (0.45- μm filter) 4 % paraformaldehyde (pH 7.4). The brains were removed and post-fixed overnight in 4 % paraformaldehyde at 4 °C followed by three 1-h washes in normal saline at 4 °C. The brains were next cryoprotected in 10 % sucrose and stored at 4 °C until they sank in the solution; they were subsequently placed in 20 % and then 30 % sucrose until they sank again in each solution. The brains were then embedded in optimal cutting temperature compound (OCT, Tissue-Tek®), and 10- μm -thick coronal serial sections were obtained. The

striatal sections (bregma 0.48 to 0.12 mm) were then selected for immunofluorescent staining. Immunolabeling protocols were applied to identify the microglial phenotypes in fresh frozen brain slices using rabbit IgG anti-Iba1 (Wako Industries, cat# 019-19741) to identify microglia/macrophages. The above primary immunoreaction was visualized using appropriate fluorophore-conjugated (Alexa Fluor dye) secondary antibodies. The cell nuclei were counterstained using 1 $\mu\text{g/ml}$ DAPI to facilitate cell counting. All fluorescence signals were imaged using an Axio Imager.Z2 upright scanning wide-field fluorescence microscope (Zeiss) equipped with an Orca Flash 4.0 high-resolution sCMOS camera (Hamamatsu), 200W X-cite 200DC broadband light source (Lumen Dynamics), and standard DAPI and Alexa Fluor filter sets (Semrock). After imaging, the image datasets were processed for image stitching and illumination correction and the images were imported into Adobe Photoshop CS6 to produce pseudo-colored composites.

Quantification

Quantification of Iba1 immunofluorescent staining was performed using FIJI image processing package, based on ImageJ (NIH, Bethesda, MD). The locations of the selected striatal, hippocampal, and cortical ROIs were identical between all the animals. The RGB bitmap images were first converted to 8-bit grayscale, and the threshold was adjusted to include only cells of interest and eliminate the background. This was followed by counting using the image-based tool for counting nuclei plug-in (ITCN). All images were processed using the same analysis parameters. The Iba1 cell density (cells/ mm^2) was calculated from the total number of positive cells divided by the total area.

Cytokine/chemokine level measurements in Tg and WT animal brain lysates

Brain lysate preparation

Cytokine/chemokine levels were measured in brain lysate solutions from two age groups, 3 month-old (five Tg and five WT) and 9 month-old (five Tg and four WT). Before sacrifice, the animals were perfused with normal saline and then were decapitated. Their brains were excised, placed into a brain matrix (World Precision Instruments, Sarasota, FL), cut into coronal section (3 mm each) and immediately frozen on dry ice then stored in -80 °C. For total protein extraction, 100-mg brain tissue sections were homogenized in 2-ml tissue extraction buffer (Novateinbio, Woburn, MA) containing protease inhibitors (Sigma, St. Louis, MO) at 1:10 dilution. After centrifugation at $19,000 \times g$ for 20 min at 4 °C, the supernatant was collected and stored in -80 °C until the assay was performed. Total protein concentration from

the supernatant was determined using BCA protein assay kit (Pierce, Rockford, IL, USA).

Tissue samples from the striatal and hippocampal areas were processed for each animal, and the samples were run in triplicates. Additional tissue samples from the cerebellum were also processed and run in duplicates. Cytokine/chemokine levels of IL-1 α , IL-1 β , IL-2, IL-4, IL-5, IL-6, IL-7, IL-10, IL-12, IL-13, IL-17, IL-18, EPO, G-CSF, GM-CSF, M-CSF, GRO/KC, MIP1 α , MIP3 α , RANTES, IFN- γ , VEGF, TNF- α , and MCP-1 were then determined using a Bio-Plex Pro™ Rat Cytokine 24-plex Assay (Bio-Rad, Hercules, CA, USA) according to the manufacturer's instructions. Concentrations of cytokine/chemokines were read on the Bio-Plex 200 System (Bio-Rad, Hercules, CA, USA).

Statistical analysis

All data are represented as mean \pm SD. Statistical significance was determined using GraphPad InStat statistical software (version 3.0, San Diego, CA, USA). For the PET scans and immunofluorescent Iba1 cell density values, the differences were compared using two-sample Student's *t* tests.

For the cytokine/chemokine data, multiple comparisons were performed using non-parametric ANOVA (Kruskal-Wallis) test followed by Dunn's post hoc analysis. Simple comparisons were made using unpaired two-tailed Student's *t* test for parametric data (with Welch correction) or Mann-Whitney *U* test for unpaired non-parametric data. A *p* value of <0.05 was considered significant.

Results

Animal weight

There were significant differences in body weight between the Tg and age-matched WT rats in the 9- ($p < 0.05$) and 16-month-old ($p < 0.01$) groups; no differences in body weight were observed in the 3-month-old group. Due to the weight differences in the adult rats, we corrected the animal weight using the Kleiber method in which the metabolic activity is proportional to $m^{0.74}$ with *m* being the animal's body weight (in grams) [30]. We chose this method as a compromise between the total body weight method of correction that could underestimate the SUV in the brain and the lean body mass method of correction that could overestimate the SUV in the brain. This method has been used in another similar paper [31].

Radiochemistry

The chemical purity of our radiotracer was consistently >95%. There were no significant differences in specific activity (SA) values nor in the injected dose (ID) of [18 F]DPA-714 in the 3-month-old (SA, 1.5 ± 0.6 and 1.3 ± 0.4 Ci/ μ mol; ID, 1.5 ± 0.3 mCi (55.5 ± 11 MBq) and

1.7 ± 0.2 mCi (62.9 ± 7.4 MBq), respectively), 9-month-old (SA, 2.1 ± 1.1 and 2.1 ± 0.9 Ci/ μ mol; ID, 1.9 ± 0.9 mCi (70.3 ± 33.3 MBq) and 1.9 ± 1.0 mCi (70.3 ± 37 MBq), respectively), or the 16-month-old Tg and age-matched WT rats (SA, 1.4 ± 0.5 and 1.4 ± 0.6 Ci/ μ mol; ID, 1.7 ± 0.1 mCi (62.9 ± 3.7 MBq) and 1.6 ± 0.1 mCi (59.2 ± 3.7 MBq), respectively). In the QA-lesioned rats, the SA was 1.6 ± 0.1 Ci/ μ mol and ID was 1.3 ± 0.4 mCi (48.1 ± 14.8 MBq).

[18 F]DPA-714 blood metabolism

No appreciable differences in blood metabolism patterns were observed between the Tg and WT rats. The parent molecule levels were similar in the Tg and WT rats at different time points: 92.40 ± 3.24 % compared to 95.81 ± 1.72 % at 5 min, 61.15 ± 22.49 % compared to 63.37 ± 15.52 % at 15 min, 35.74 ± 11.92 % compared to 37.14 ± 8.00 % at 30 min and 20.31 ± 4.97 % compared to 25.79 ± 6.70 % at 60 min (Fig. 1). Our metabolism results were very similar to previously reported values in the literature [32].

[18 F]DPA-714 PET

The time-activity curves (TACs) of the 60-min acquisitions were similar in shape between the Tg and WT rats in all regions. Representative TACs derived from the caudate nucleus region are shown in Fig. 2 and Additional file 1. The radioligand was rapidly taken up in the brain but displayed fast washout with only small activity concentrations measured at later time points. Pseudo equilibrium was reached at approximately 40 min after injection (Fig. 2).

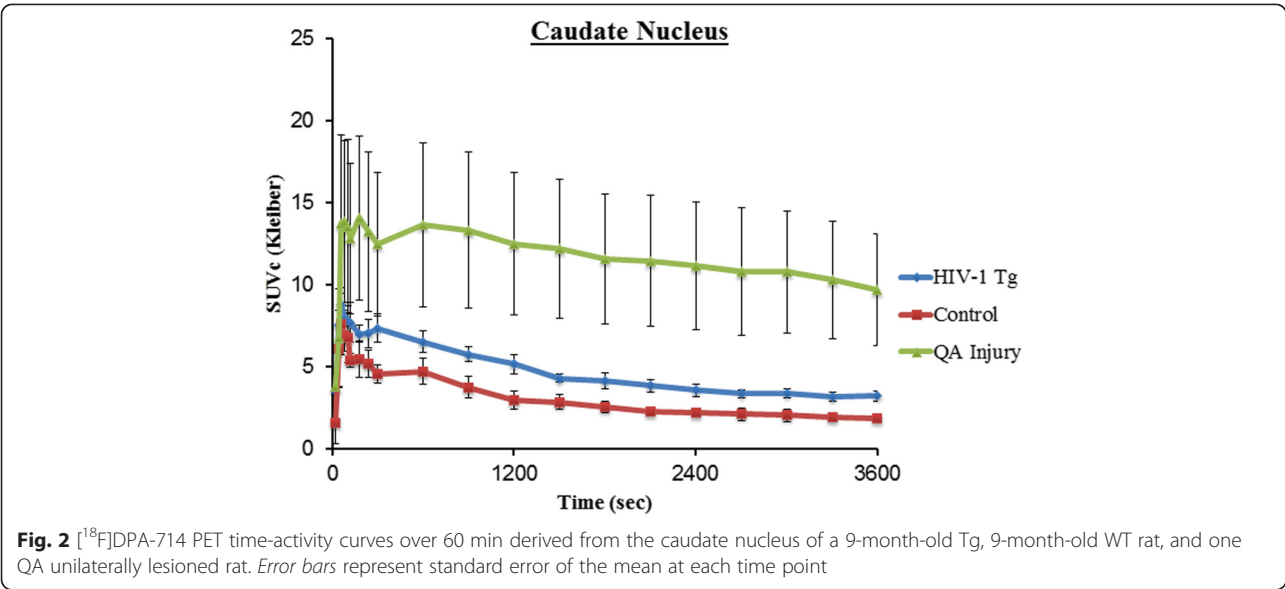
In all the three age groups, the Tg rats generally showed slightly increased SUV values compared to the age-matched WT rats; however, this was not statistically significant in any group or any brain region (Table 1, Fig. 3b, c). In the QA-injected rats, on the other hand, there was a definite increase in [18 F]DPA-714 binding ipsilateral to the injection site when compared to the contralateral side (Fig. 3a). The increased uptake was seen in the caudate at the site of the injection as well as along the tract of the needle in the cortex. The fold increase ranged from 1.2 to 2 (ipsilateral versus contralateral ratio).

Immunofluorescence

The Iba1 cell density values (cells/mm²) were not significantly different between the Tg and WT rats in any of the evaluated brain regions, which included the cortex, striatum, and hippocampus (two-sample Student's *t* test, $p > 0.05$).

Cytokine/chemokine measurements in the brain lysates

For all the measured cytokine/chemokines in the brain lysates, there were no significant differences in cytokine/



chemokine concentrations between the Tg and age-matched WT animals at any age (Fig. 4). When we compared the general direction of change with age between the TG and WT rats, there were no appreciable differences with cytokine/chemokine concentrations generally following the same pattern of either increase, decrease, or no change in both groups.

Discussion

The exact neuropathology leading to milder forms of HIV-associated neurocognitive disorders (HAND) is not fully understood. Unlike microglia and astrocytes, neurons do not express CD4 and there is no direct evidence of productively infected neurons with HIV [33, 34]. The neurologic damage is rather thought related to persistent low level of neuroinflammation [5, 35], neurotoxic effects of viral proteins [36, 37], as well as the indirect disruption of the supportive and neurotrophic role of astrocytes [38] and oligodendrocytes [39]. Among those factors, the contribution of neuroinflammation (microglial activation) to neuronal damage is believed to play a major role [8, 5, 6, 4, 7, 3]. As a result, there were three attempts to image microglial activation in vivo in

HIV-positive (HIV+) patients using PET. All three groups [40–42] used [¹¹C]PK11195; however, the results were inconsistent, which is probably due to the heterogeneity of patient populations, as far as treatment and neurological status, as well as the limitations of [¹¹C]PK11195 as a radiotracer [17–20]. One way of controlling for those variables is to perform imaging studies in animal models. The Tg rat is a non-infectious small animal model of HIV infection, in which the expression of the transgene, consisting of an HIV-1 provirus with functional deletion of gag and pol, is regulated by the viral long terminal repeat [43]. There is no potential for replication, but there is chronic exposure to viral proteins, such as Tat, gp120, Vpr, and Nef. The HIV-1 Tg rat exhibits pathologies and immune irregularities characteristic of HIV-1 infection of humans. As a model for HIV infection, it was found to develop consistent neurological and behavioral deficits [44–47], increased expression of microglial markers such as CD11b, and, with some groups [48, 35, 49], but not others [50], increased levels of multiple cytokines and chemokines. It thus appears to be of particular importance for the evaluation of neurological complications of HIV. The non-

Table 1 Corrected standardized uptake values (SUVc = % ID. kg/cm³) for Tg and age-matched WT rats at three age groups

Region	3-month-old			9-month-old			16-month-old		
	Tg	WT	p value	Tg	WT	p value	Tg	WT	p value
Cortex	3.07 ± 0.23	2.87 ± 0.79	0.65	2.81 ± 0.71	2.32 ± 0.42	0.21	2.19 ± 0.43	1.61 ± 0.29	0.1
Caudate	2.62 ± 0.18	2.68 ± 0.87	0.90	2.60 ± 0.62	2.02 ± 0.41	0.11	2.18 ± 0.53	1.58 ± 0.22	0.11
Thalamus	2.32 ± 0.27	2.12 ± 0.45	0.47	2.51 ± 0.66	2.06 ± 0.38	0.22	1.98 ± 0.50	1.42 ± 0.14	0.11
Hippocampus	2.35 ± 0.38	2.14 ± 0.47	0.50	3.41 ± 0.60	2.54 ± 0.79	0.1	1.93 ± 0.63	1.40 ± 0.17	0.21
Cerebellum	3.40 ± 0.17	3.14 ± 0.80	0.54	3.37 ± 1.00	2.94 ± 0.62	0.42	2.60 ± 0.71	1.90 ± 0.22	0.15

Values are listed as mean SUVc ± SD for each group

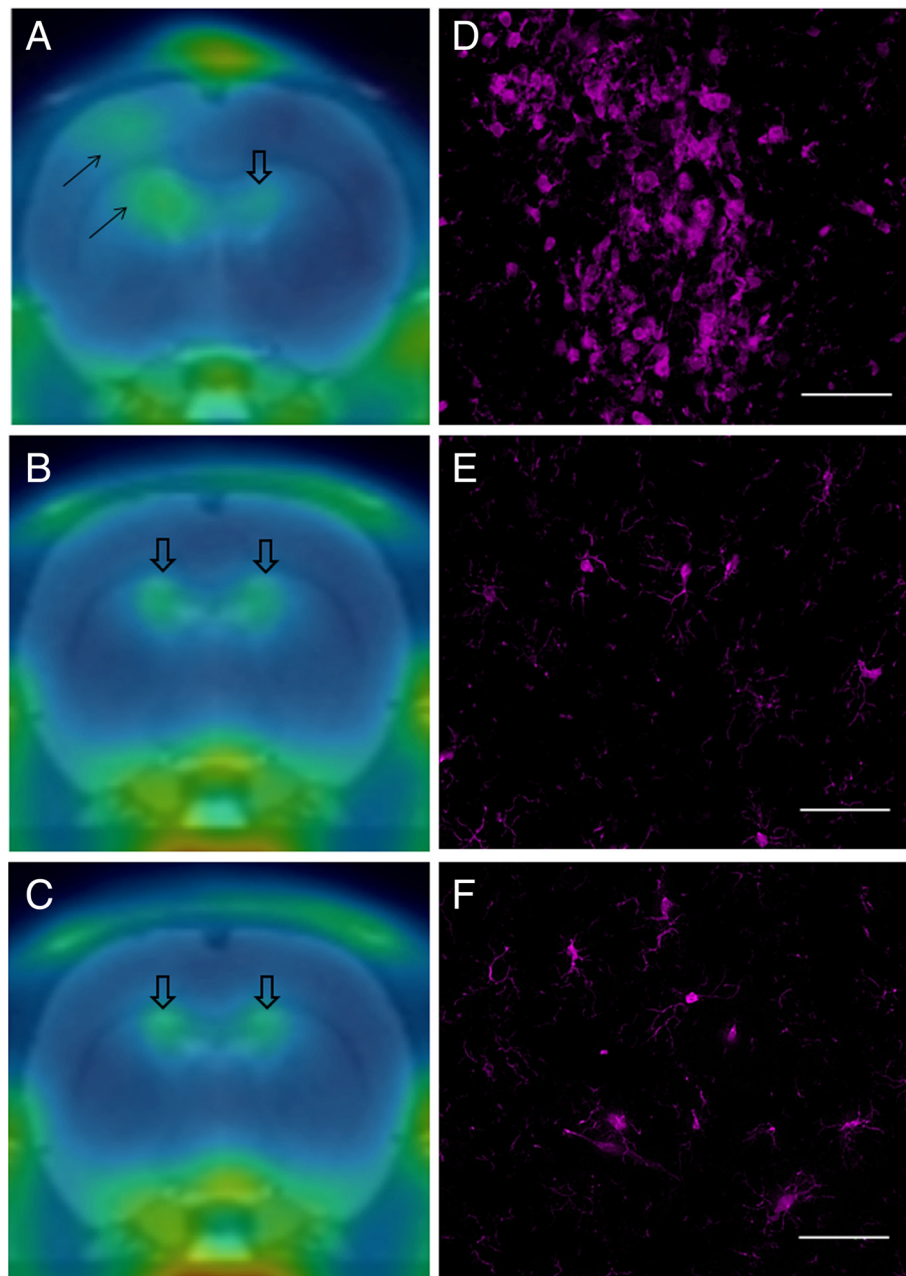


Fig. 3 Representative coronal [^{18}F]DPA-714 PET summed images between 40 and 60 min of acquisition in **a** QA-injected rat, **b** 9-month-old Tg, and **c** 9-month-old WT rat, in template MRI stereotaxic space. Increased [^{18}F]DPA-714 uptake is seen ipsilateral to the QA injury site in **a** (solid black arrows). No qualitative differences in uptake between the Tg and WT rats are seen. Areas of uptake in **a**, **b**, and **c** (open arrows) are due to normal [^{18}F]DPA-714 PET uptake in the choroid plexus within the ventricular system. Intense Iba1 immunofluorescent staining (increased size and number of activated microglia) in the QA-lesioned rat (**d**), with comparable staining of cells in middle-aged Tg (**e**) and age-matched WT (**f**) rats (scale bar 100 μm)

infectious nature of the model, the larger brain size allowing for microPET imaging (compared to mice) and the commercial availability of the Tg rat are additional positive factors. In our study, we set out to validate [^{18}F]DPA-714 as an *in vivo* biomarker of microglial activation in the Tg rat so that we can ultimately use the combination of the

animal model and ligand in the evaluation of the effectiveness of neuroprotective therapies/approaches.

[^{18}F]DPA-714 has been useful in the study of other animal models of neuroinflammation including encephalitis [18], cerebral ischemia [20, 51], epilepsy [52], excitotoxicity [53], glioma [32, 54, 55] and other preclinical

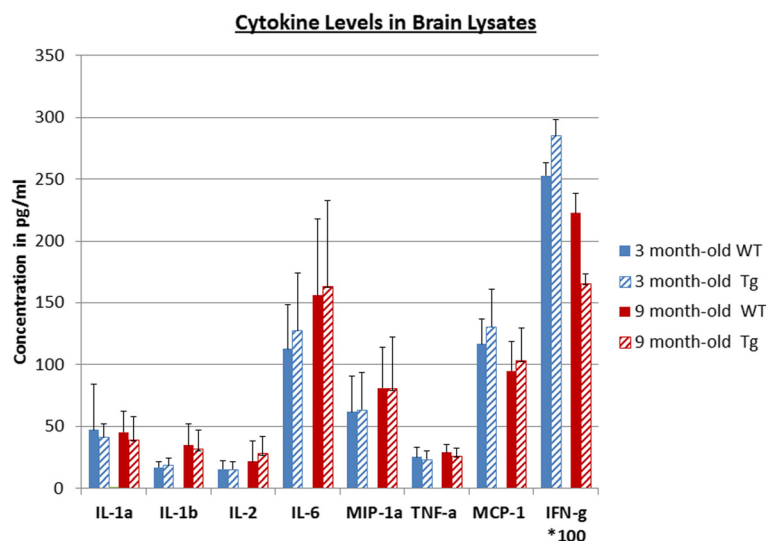


Fig. 4 Brain lysate concentrations of select cytokine/chemokines in Tg and WT rats, at two age groups (3 and 9 months old). There were no statistically significant differences in cytokine/chemokine levels between the Tg and WT animals at any age

neurodegenerative disease models. Useful neuroimaging probes should fulfill a number of key general properties: appropriate lipophilicity, lack of toxicity, small size with high selectivity for the target site, and preferably lack of radiolabeled metabolites that can cross the blood brain barrier. With PET ligands, however, differences in cerebral metabolism have been described in genetically engineered small animal models and/or pathologically modified rodents [56]. Therefore, since we are dealing with a transgenic animal model, we evaluated plasma [^{18}F]DPA-714 metabolism and found no difference between the Tg and WT rats, with similar clearance rates of the ligand from the blood in both groups.

We chose to evaluate three different age groups (young, middle-aged, and old) because we assumed the older animals would demonstrate more neuroinflammation by virtue of longer exposure to viral proteins. We also based our choice on other functional and structural abnormalities that we previously detected in the Tg rats at those ages and that worsened with aging [57, 58]. Using [^{18}F]DPA-714, we found higher mean SUV_c values in the Tg rats compared to the age-matched WT rats; however, this difference did not reach statistical significance in any region or age group. In the unilateral QA striatal injection model (known to induce inflammation and increased TSPO expression [19]), on the other hand, there was clear increased uptake in the ipsilateral striatum (Fig. 3a). Immunofluorescent staining confirmed the *in vivo* findings with no qualitatively appreciable difference in Iba1 cellular counts in the Tg brains compared to age-matched WT rats (Fig. 3e, f). Microglial activation on the other hand was clearly demonstrated

in the QA-lesioned rat brains, ipsilateral to the injection site/needle tract (Fig. 3d).

To further support our findings, we measured the concentrations of 24 cytokine/chemokines in the brain lysates of the Tg and WT animals at two different ages: 3 and 9 months. This was of relevance since the literature was not consistent about this topic: while some groups detected increased cytokine/chemokines [35, 59], others did not [50]. In our hands, there were no significant differences in cytokine/chemokine concentrations in brain lysates between the Tg and WT rats at either age (Fig. 4).

One limitation of our study is that direct estimation of specific binding was not possible since there is no suitable reference region available for TSPO binding in this model with diffuse neuropathology, and arterial blood sampling is not logistically feasible. In such cases, it is not unusual to perform qualitative comparison of the regional distribution of the tracer (SUV) in the different groups of animals if the studies are run in parallel. In fact, other researchers have previously used SUV quantification with [^{18}F]DPA-714, with success [54, 60–62]. We were also encouraged to use SUV by a recent paper that found significant correlation between SUV values and distribution volume measurements in rat brains using a similar TSPO ligand [63]. Unfortunately, a similar comparison has not been done using [^{18}F]DPA-714 in rats. Another inherent limitation of the model of our study is the discrepancy in weight between the Tg and WT animals as they grow older. To minimize the effect associated with this discrepancy, we decided to correct SUV values for weight differences [30, 31].

In conclusion, even though the HIV-1Tg rat is a good animal model of viral protein neurotoxicity and treated HIV+ patients [46, 49, 59, 64, 65], we did not find appreciable microglial activation to allow the use of [^{18}F]DPA-714 PET imaging as a biomarker of neurodegeneration in the evaluation of existing and emerging neuroprotective therapies. Alternative imaging targets relevant to the neuropathology of the Tg rat should thus be sought, such as those related to oxidative stress [66–69], arachidonic acid metabolism [48], NMDA excitotoxicity, abnormal dopamine receptor signaling/tyrosine metabolism [57, 70], abnormal myelination [70], and astrocytic death [58].

Additional file

Additional file 1: Figure S1. [^{18}F]DPA-714 PET time-activity curves over 60 min derived from the caudate and hippocampus of 3-, 6-, and 9-month-old Tg and WT rats. Error bars represent standard deviation values at each time point. (TIFF 2460 kb)

Abbreviations

ACUC: Animal Care and Use Committee; ART: antiretroviral therapy; HAND: HIV-associated neurocognitive disorders; ID: injected dose; NIH: National Institutes of Health; PET: positron emission tomography; QA: quinolinic acid; SA: specific activity; Tg: HIV-1 transgenic rat; TLC: thin layer chromatography; TSPO: translocator protein; WT: wild type.

Competing interests

The authors declare that they have no competing interests.

Authors' contributions

DL performed the microPET experiments, analyzed the data, performed the statistical analysis, prepared the table and figures, and drafted the first version of the manuscript. XY performed the radiochemical synthesis of the ligand, performed all the quality control steps, and provided the methods section on radiochemical synthesis. WI analyzed the immunofluorescence slides on all animals, performed the cytokine/chemokine measurements, and performed associated statistical analysis. ML, KP, and EJ performed the biodistribution studies with metabolites' analysis and performed all associated quantifications. They also assisted with performing the microPET scans. MK provided the precursor for the DPA ligand, reviewed the radiochemical synthesis for integrity, and performed a critical review of the manuscript. DM performed all the immunofluorescent staining procedures and image processing. WR helped with study and protocol design, assisted with the Bio-Plex experiments and microPET experiments, and performed the animal euthanasia and brain tissue preparations. DH conceived the study, designed the imaging protocol, qualitatively analyzed the immunofluorescent sections, prepared the table and figures, and provided the last draft of the manuscript. All authors read and approved the final manuscript.

Acknowledgments

This work was supported by the Center of Infectious Disease Imaging (CIDI), Radiology and Imaging Sciences (RIS), Clinical Center, National Institutes of Health (Intramural Program).

Author details

¹Center for Infectious Disease Imaging (CIDI), Radiology and Imaging Sciences, National Institutes of Health/Clinical Center, 10 Center Drive, Room 1C368, Bethesda, MD 20814-9692, USA. ²Department of Radiology, Washington University School of Medicine, St. Louis, MO, USA. ³Molecular Imaging Program (MIP), National Cancer Institute (NCI), Bethesda, MD, USA. ⁴Chemistry Department, The University of Sydney, Sydney, Australia. ⁵Division of Intramural Research (DIR), National Institute of Neurological Disorders and Stroke (NINDS), National Institutes of Health, Bethesda, MD, USA.

Received: 11 July 2015 Accepted: 2 September 2015

Published online: 17 September 2015

References

- McArthur JC, Steiner J, Sacktor N, Nath A. Human immunodeficiency virus-associated neurocognitive disorders: mind the gap. *Ann Neurol*. 2010;67(6):699–714.
- Tan IL, McArthur JC. HIV-associated neurological disorders: a guide to pharmacotherapy. *CNS drugs*. 2012;26(2):123–34. doi:10.2165/11597770-000000000-00000.
- Venneti S, Lopresti BJ, Wiley CA. The peripheral benzodiazepine receptor (translocator protein 18 kDa) in microglia: from pathology to imaging. *Prog Neurobiol*. 2006;80(6):308–22.
- Lu SM, Tremblay ME, King IL, Qi J, Reynolds HM, Marker DF, et al. HIV-1 Tat-induced microglial and synaptic damage via interactions between peripheral and central myeloid cells. *PLoS One*. 2011;6(9):e23915.
- Guha D, Nagilla P, Redinger C, Srinivasan A, Schatten GP, Ayyavoo V. Neuronal apoptosis by HIV-1 Vpr: contribution of proinflammatory molecular networks from infected target cells. *J Neuroinflammation*. 2012;9:138. doi:10.1186/1742-2094-9-138.
- Kramer-Hammerle S, Rothenaigner I, Wolff H, Bell JE, Brack-Werner R. Cells of the central nervous system as targets and reservoirs of the human immunodeficiency virus. *Virus Res*. 2005;111(2):194–213. doi:10.1016/j.virusres.2005.04.009.
- Renner NA, Sansing HA, Morici LA, Inglis FM, Lackner AA, MacLean AG. Microglia activation by SIV-infected macrophages: alterations in morphology and cytokine secretion. *J Neurovirol*. 2012;18(3):213–21. doi:10.1007/s13365-012-0100-7.
- Cosenza-Nashat M, Zhao ML, Suh HS, Morgan J, Natividad R, Morgello S, et al. Expression of the translocator protein of 18 kDa by microglia, macrophages and astrocytes based on immunohistochemical localization in abnormal human brain. *Neuropathol Appl Neurobiol*. 2009;35(3):306–28. doi:10.1111/j.1365-2990.2008.01006.x.
- Scaff AM, Kassou M. The translocator protein. *J Nucl Med*. 2011;52(5):677–80.
- Dheen ST, Kaur C, Ling EA. Microglial activation and its implications in the brain diseases. *Curr Med Chem*. 2007;14(11):1189–97.
- Cagnin A, Kassou M, Meikle SR, Banati RB. In vivo evidence for microglial activation in neurodegenerative dementia. *Acta Neurol Scand Suppl*. 2006;185:107–14.
- Banati RB, Newcombe J, Gunn RN, Cagnin A, Turkheimer F, Heppner F, et al. The peripheral benzodiazepine binding site in the brain in multiple sclerosis: quantitative in vivo imaging of microglia as a measure of disease activity. *Brain*. 2000;123(Pt 11):2321–37.
- Cagnin A, Myers R, Gunn RN, Lawrence AD, Stevens T, Kreutzberg GW, et al. In vivo visualization of activated glia by [^{11}C] (R)-PK11195-PET following herpes encephalitis reveals projected neuronal damage beyond the primary focal lesion. *Brain*. 2001;124(Pt 10):2014–27.
- Tai YF, Pavese N, Gerhard A, Tabrizi SJ, Barker RA, Brooks DJ, et al. Imaging microglial activation in Huntington's disease. *Brain Res Bull*. 2007;72(2–3):148–51.
- Gerhard A, Trender-Gerhard I, Turkheimer F, Quinn NP, Bhatia KP, Brooks DJ. In vivo imaging of microglial activation with [^{11}C] (R)-PK11195 PET in progressive supranuclear palsy. *Mov Disord*. 2006;21(1):89–93.
- Gerhard A, Watts J, Trender-Gerhard I, Turkheimer F, Banati RB, Bhatia K, et al. In vivo imaging of microglial activation with [^{11}C] (R)-PK11195 PET in corticobasal degeneration. *Mov Disord*. 2004;19(10):1221–6.
- Chauveau F, Van Camp N, Dolle F, Kuhnast B, Hinnen F, Damont A, et al. Comparative evaluation of the translocator protein radioligands 11C-DPA-713, 18F-DPA-714, and 11C-PK11195 in a rat model of acute neuroinflammation. *J Nucl Med*. 2009;50(3):468–76.
- Doorduyn J, Klein HC, Dierckx RA, James M, Kassou M, de Vries EF. [^{11}C] DPA-713 and [^{18}F] DPA-714 as new PET tracers for TSPO: a comparison with [^{11}C] (R)-PK11195 in a rat model of herpes encephalitis. *Mol Imaging Biol*. 2009;11(6):386–98.
- James ML, Fulton RR, Vercoullie J, Henderson DJ, Garreau L, Chalon S, et al. DPA-714, a new translocator protein-specific ligand: synthesis, radiofluorination, and pharmacological characterization. *J Nucl Med*. 2008;49(5):814–22.
- Martin A, Boisgard R, Theze B, Van Camp N, Kuhnast B, Damont A, et al. Evaluation of the PBR/TSPO radioligand [^{18}F] DPA-714 in a rat model of focal cerebral ischemia. *J Cereb Blood Flow Metab*. 2010;30(1):230–41.

21. Endres CJ, Pomper MG, James M, Uzuner O, Hammoud DA, Watkins CC, et al. Initial evaluation of ¹¹C-DPA-713, a novel TSPO PET ligand, in humans. *J Nucl Med*. 2009;50(8):1276–82.
22. Brown AK, Fujita M, Fujimura Y, Liow JS, Stabin M, Ryu YH, et al. Radiation dosimetry and biodistribution in monkey and man of ¹¹C-PBR28: a PET radioligand to image inflammation. *J Nucl Med*. 2007;48(12):2072–9.
23. Arlicot N, Katsifis A, Garreau L, Mattner F, Vergote J, Duval S, et al. Evaluation of CLINDE as potent translocator protein (18 kDa) SPECT radiotracer reflecting the degree of neuroinflammation in a rat model of microglial activation. *Eur J Nucl Med Mol Imaging*. 2008;35(12):2203–11.
24. Mattner F, Bandin DL, Staykova M, Berghofer P, Gregoire MC, Ballantyne P, et al. Evaluation of [(1)(2)(3)]-CLINDE as a potent SPECT radiotracer to assess the degree of astroglia activation in cuprizone-induced neuroinflammation. *Eur J Nucl Med Mol Imaging*. 2011;38(8):1516–28.
25. Venneti S, Wang G, Wiley CA. The high affinity peripheral benzodiazepine receptor ligand DAA1106 binds to activated and infected brain macrophages in areas of synaptic degeneration: implications for PET imaging of neuroinflammation in lentiviral encephalitis. *Neurobiol Dis*. 2008;29(2):232–41.
26. Martin A, Boisgard R, Kassiou M, Dolle F, Tavitian B. Reduced PBR/TSPO expression after minocycline treatment in a rat model of focal cerebral ischemia: a PET study using [(18)F]DPA-714. *Mol Imaging Biol*. 2011;13(1):10–5.
27. Schweinhardt P, Fransson P, Olson L, Spenger C, Andersson JL. A template for spatial normalisation of MR images of the rat brain. *J Neurosci Methods*. 2003;129(2):d105–13.
28. Paxinos G, Watson C. *The Rat Brain: In Stereotaxic Coordinates*. Academic Press, Incorporated: London, UK; 1998.
29. Lee DE, Gallezot JD, Zheng MQ, Lim K, Ding YS, Huang Y, et al. Test-retest reproducibility of [¹¹C]-(+)-propyl-hexahydro-naphtho-oxazin positron emission tomography using the bolus plus constant infusion paradigm. *Mol Imaging*. 2013;12(2):77–82.
30. Kleiber M. Body size and metabolic rate. *Physiol Rev*. 1947;27(4):511–41.
31. Drake C, Boutin H, Jones MS, Denes A, McColl BW, Selvarajah JR, et al. Brain inflammation is induced by co-morbidities and risk factors for stroke. *Brain Behav Immun*. 2011;25(6):1113–22. doi:10.1016/j.bbi.2011.02.008.
32. Tang D, Hight MR, McKinley ET, Fu A, Buck JR, Smith RA, et al. Quantitative preclinical imaging of TSPO expression in glioma using N, N-diethyl-2-(2-(4-(2-18F-fluoroethoxy)phenyl)-5,7-dimethylpyrazolo[1,5-a]pyrimidin-3-yl)acetamide. *J Nucl Med*. 2012;53(2):287–94. doi:10.2967/jnumed.111.095653.
33. Mocchetti I, Bachis A, Avdoshina V. Neurotoxicity of human immunodeficiency virus-1: viral proteins and axonal transport. *Neurotox Res*. 2011. doi:10.1007/s12640-011-9279-2.
34. Kovalevich J, Langford D. Neuronal toxicity in HIV CNS disease. *Futur Virol*. 2012;7(7):687–98. doi:10.2217/fvl.1257.
35. Rao JS, Kim HW, Kellom M, Greenstein D, Chen M, Kraft AD, et al. Increased neuroinflammatory and arachidonic acid cascade markers, and reduced synaptic proteins, in brain of HIV-1 transgenic rats. *J Neuroinflammation*. 2011;8(1):101.
36. Agrawal L, Louboutin JP, Reyes BA, Van Bockstaele EJ, Strayer DS. HIV-1 Tat neurotoxicity: a model of acute and chronic exposure, and neuroprotection by gene delivery of antioxidant enzymes. *Neurobiol Dis*. 2012;45(2):657–70. doi:10.1016/j.nbd.2011.10.005.
37. Hu S, Sheng WS, Lokensgard JR, Peterson PK, Rock RB. Preferential sensitivity of human dopaminergic neurons to gp120-induced oxidative damage. *J Neurovirol*. 2009;15(5–6):401–10.
38. Bezzi P, Domercq M, Brambilla L, Galli R, Schols D, De Clercq E, et al. CXCR4-activated astrocyte glutamate release via TNF α : amplification by microglia triggers neurotoxicity. *Nat Neurosci*. 2001;4(7):702–10. doi:10.1038/89490.
39. Radja F, Kay DG, Albrecht S, Jolicœur P. Oligodendrocyte-specific expression of human immunodeficiency virus type 1 Nef in transgenic mice leads to vacuolar myelopathy and alters oligodendrocyte phenotype in vitro. *J Virol*. 2003;77(21):11745–53.
40. Garvey LJ, Pavese N, Politis M, Ramlackhansingh A, Brooks DJ, Taylor-Robinson SD et al. Increased microglia activation in neurologically asymptomatic HIV-infected patients receiving effective ART; An ¹¹C-PK11195 PET study. *AIDS (London, England)*. 2013. doi:10.1097/01.aids.0000432467.54003.f7.
41. Hammoud DA, Endres CJ, Chander AR, Guilarte TR, Wong DF, Sacktor NC, et al. Imaging glial cell activation with [¹¹C]-R-PK11195 in patients with AIDS. *J Neurovirol*. 2005;11(4):346–55.
42. Wiley CA, Lopresti BJ, Becker JT, Boada F, Lopez OL, Mellors J, et al. Positron emission tomography imaging of peripheral benzodiazepine receptor binding in human immunodeficiency virus-infected subjects with and without cognitive impairment. *J Neurovirol*. 2006;12(4):262–71.
43. Reid W, Sadowska M, Denaro F, Rao S, Foulke Jr J, Hayes N, et al. An HIV-1 transgenic rat that develops HIV-related pathology and immunologic dysfunction. *Proc Natl Acad Sci U S A*. 2001;98(16):9271–6.
44. Lashomb AL, Vigorito M, Chang SL. Further characterization of the spatial learning deficit in the human immunodeficiency virus-1 transgenic rat. *J Neurovirol*. 2009;15(1):14–24.
45. Moran LM, Booze RM, Mactutus CF. Modeling deficits in attention, inhibition, and flexibility in HAND. *J Neuroimmune Pharmacol*. 2014;9(4):508–21. doi:10.1007/s11481-014-9539-z.
46. Vigorito M, Connaghan KP, Chang SL. The HIV-1 transgenic rat model of neuroHIV. *Brain Behav Immun*. 2015. doi:10.1016/j.bbi.2015.02.020.
47. Wayman WN, Chen L, Persons AL, Napier TC. Cortical consequences of HIV-1 Tat exposure in rats are enhanced by chronic cocaine. *Curr HIV Res*. 2015;13(1):80–7.
48. Basselin M, Ramadan E, Igarashi M, Chang L, Chen M, Kraft AD, et al. Imaging upregulated brain arachidonic acid metabolism in HIV-1 transgenic rats. *J Cereb Blood Flow Metab*. 2011;31(2):486–93.
49. Repunte-Canonigo V, Lefebvre C, George O, Kawamura T, Morales M, Koob GF, et al. Gene expression changes consistent with neuroAIDS and impaired working memory in HIV-1 transgenic rats. *Mol Neurodegener*. 2014;9:26. doi:10.1186/1750-1326-9-26.
50. Homji NF, Mao X, Langsdorf EF, Chang SL. Endotoxin-induced cytokine and chemokine expression in the HIV-1 transgenic rat. *J Neuroinflammation*. 2012;9:3. doi:10.1186/1742-2094-9-3.
51. Boutin H, Prenant C, Maroy R, Galea J, Greenhalgh AD, Smigova A et al. [¹⁸F]DPA-714: direct comparison with [¹¹C]PK11195 in a model of cerebral ischemia in rats. *PLoS One*. 2013;8(2):e56441. doi:10.1371/journal.pone.0056441.
52. Harhausen D, Sudmann V, Khojasteh U, Muller J, Zille M, Graham K, et al. Specific imaging of inflammation with the 18 kDa translocator protein ligand DPA-714 in animal models of epilepsy and stroke. *PLoS One*. 2013;8(8):e69529. doi:10.1371/journal.pone.0069529.
53. Lavisse S, Guillemier M, Herard AS, Petit F, Delahaye M, Van Camp N, et al. Reactive astrocytes overexpress TSPO and are detected by TSPO positron emission tomography imaging. *J Neurosci*. 2012;32(32):10809–18. doi:10.1523/jneurosci.1487-12.2012.
54. Awde AR, Boisgard R, Theze B, Dubois A, Zheng J, Dolle F, et al. The translocator protein radioligand ¹⁸F-DPA-714 monitors antitumor effect of erufosine in a rat 9L intracranial glioma model. *J Nucl Med*. 2013;54(12):2125–31. doi:10.2967/jnumed.112.118794.
55. Winkler A, Boisgard R, Awde AR, Dubois A, Theze B, Zheng J, et al. The translocator protein ligand [(1)(8)F]DPA-714 images glioma and activated microglia in vivo. *Eur J Nucl Med Mol Imaging*. 2012;39(5):811–23. doi:10.1007/s00259-011-2041-4.
56. Smith G. Animal models of Alzheimer's disease: experimental cholinergic denervation. *Brain Res*. 1988;472(2):103–18.
57. Lee DE, Reid WC, Ibrahim WG, Peterson KL, Lentz MR, Maric D, et al. Imaging dopaminergic dysfunction as a surrogate marker of neuropathology in a small-animal model of HIV. *Mol Imaging*. 2014;13:1–10.
58. Lentz MR, Peterson KL, Ibrahim WG, Lee DE, Sarlis J, Lizak MJ, et al. Diffusion tensor and volumetric magnetic resonance measures as biomarkers of brain damage in a small animal model of HIV. *PLoS One*. 2014;9(8):e105752. doi:10.1371/journal.pone.0105752.
59. Royal 3rd W, Zhang L, Guo M, Jones O, Davis H, Bryant JL. Immune activation, viral gene product expression and neurotoxicity in the HIV-1 transgenic rat. *J Neuroimmunol*. 2012;247(1–2):16–24. doi:10.1016/j.jneuroim.2012.03.015.
60. Doorduyn J, de Vries EF, Dierckx RA, Klein HC. PET imaging of the peripheral benzodiazepine receptor: monitoring disease progression and therapy response in neurodegenerative disorders. *Curr Pharm Des*. 2008;14(31):3297–315.
61. Vicidomini C, Panico M, Greco A, Gargiulo S, Coda AR, Zannetti A, et al. In vivo imaging and characterization of [(18)F]DPA-714, a potential new TSPO ligand, in mouse brain and peripheral tissues using small-animal PET. *Nucl Med Biol*. 2015;42(3):309–16. doi:10.1016/j.nucmedbio.2014.11.009.
62. Zinnhardt B, Viel T, Wachsmuth L, Vrachimis A, Wagner S, Breyholz HJ, et al. Multimodal imaging reveals temporal and spatial microglia and matrix

- metalloproteinase activity after experimental stroke. *J Cereb Blood Flow Metab.* 2015. doi:10.1038/jcbfm.2015.149.
63. Toth M, Doorduyn J, Haggkvist J, Varrone A, Amini N, Halldin C, et al. Positron emission tomography studies with [¹¹C]PBR28 in the healthy rodent brain: validating SUV as an outcome measure of neuroinflammation. *PLoS One.* 2015;10(5):e0125917. doi:10.1371/journal.pone.0125917.
 64. Moran LM, Booze RM, Webb KM, Mactutus CF. Neurobehavioral alterations in HIV-1 transgenic rats: evidence for dopaminergic dysfunction. *Exp Neurol.* 2013;239:139–47. doi:10.1016/j.expneurol.2012.10.008.
 65. Peng J, Vigorito M, Liu X, Zhou D, Wu X, Chang SL. The HIV-1 transgenic rat as a model for HIV-1 infected individuals on HAART. *J Neuroimmunol.* 2010;218(1–2):94–101.
 66. Blanchard HC, Taha AY, Rapoport SI, Yuan ZX. Low-dose aspirin (acetylsalicylate) prevents increases in brain PGE₂, 15-epi-lipoxin A₄ and 8-isoprostane concentrations in 9 month-old HIV-1 transgenic rats, a model for HIV-1 associated neurocognitive disorders. *Prostaglandins Leukot Essent Fat Acids.* 2015;96:25–30. doi:10.1016/j.plefa.2015.01.002.
 67. Davinelli S, Scapagnini G, Denaro F, Calabrese V, Benedetti F, Krishnan S, et al. Altered expression pattern of Nrf2/HO-1 axis during accelerated-senescence in HIV-1 transgenic rat. *Biogerontology.* 2014;15(5):449–61. doi:10.1007/s10522-014-9511-6.
 68. Pang X, Panee J. Roles of glutathione in antioxidant defense, inflammation, and neuron differentiation in the thalamus of HIV-1 transgenic rats. *J Neuroimmune Pharmacol.* 2014;9(3):413–23. doi:10.1007/s11481-014-9538-0.
 69. Walker MD, Dinelle K, Kornelsen R, Lee NV, Miao Q, Adam M et al. [¹¹C]PBR28 PET imaging is sensitive to neuroinflammation in the aged rat. *J Cereb Blood Flow Metab.* 2015. doi:10.1038/jcbfm.2015.54.
 70. Li MD, Cao J, Wang S, Wang J, Sarkar S, Vigorito M, et al. Transcriptome sequencing of gene expression in the brain of the HIV-1 transgenic rat. *PLoS One.* 2013;8(3):e59582. doi:10.1371/journal.pone.0059582.

**Submit your next manuscript to BioMed Central
and take full advantage of:**

- Convenient online submission
- Thorough peer review
- No space constraints or color figure charges
- Immediate publication on acceptance
- Inclusion in PubMed, CAS, Scopus and Google Scholar
- Research which is freely available for redistribution

Submit your manuscript at
www.biomedcentral.com/submit

